A&A 564, A60 (2014)
DOI: 10.1051/0004-6361/201323321

Astronomy & Astrophysics

The extreme chemistry of multiple stellar populations in the metal-poor globular cluster NGC 4833⋆,⋆⋆

E. Carretta[1], A. Bragaglia[1], R. G. Gratton[2], V. D'Orazi[3,4], S. Lucatello[2], Y. Momany[2,5], A. Sollima[1], M. Bellazzini[1], G. Catanzaro[6], and F. Leone[7]

[1] INAF – Osservatorio Astronomico di Bologna, via Ranzani 1, 40127 Bologna, Italy
e-mail: eugenio.carretta@oabo.inaf.it
[2] INAF – Osservatorio Astronomico di Padova, Vicolo dell'Osservatorio 5, 35122 Padova, Italy
[3] Dept. of Physics and Astronomy, Macquarie University, NSW 2109 Sydney, Australia
[4] Monash Centre for Astrophysics, Monash University, School of Mathematical Sciences, Building 28, VIC 3800 Clayton, Melbourne, Australia
[5] European Southern Observatory, Alonso de Cordova 3107, Casilla 19001, Vitacura, Santiago, Chile
[6] INAF-Osservatorio Astrofisico di Catania, via S. Sofia 78, 95123 Catania, Italy
[7] Dipartimento di Fisica e Astronomia, Università di Catania, via S. Sofia 78, 95123 Catania, Italy

Received 23 December 2013 / Accepted 27 January 2014

ABSTRACT

Our FLAMES survey of Na-O anticorrelation in globular clusters (GCs) is extended to NGC 4833, a metal-poor GC with a long blue tail on the horizontal branch (HB). We present the abundance analysis for a large sample of 78 red giants based on UVES and GIRAFFE spectra acquired at the ESO-VLT. We derived abundances of Na, O, Mg, Al, Si, Ca, Sc, Ti, V, Cr, Mn, Fe, Co, Ni, Cu, Zn, Y, Ba, La, and Nd. This is the first extensive study of this cluster from high resolution spectroscopy. On the scale of our survey, the metallicity of NGC 4833 is [Fe/H] = $-2.015 \pm 0.004 \pm 0.084$ dex (rms = 0.014 dex) from 12 stars observed with UVES, where the first error is from statistics and the second one refers to the systematic effects. The iron abundance in NGC 4833 is homogeneous at better than 6%. On the other hand, the light elements involved in proton-capture reactions at high temperature show the large star-to-star variations observed in almost all GCs studied so far. The Na-O anticorrelation in NGC 4833 is quite extended, as expected from the high temperatures reached by stars on the HB, and NGC 4833 contains a conspicuous fraction of stars with extreme [O/Na] ratios. More striking is the finding that large star-to-star variations are also seen for Mg, which spans a range of more than 0.5 dex in this GC. Depletions in Mg are correlated to the abundances of O and anti-correlated with Na, Al, and Si abundances. This pattern suggests the action of nuclear processing at unusually high temperatures, producing the extreme chemistry observed in the stellar generations of NGC 4833. These extreme changes are also seen in giants of the much more massive GCs M 54 and ω Cen, and our conclusion is that NGC 4833 has probably lost a conspicuous fraction of its original mass due to bulge shocking, as also indicated by its orbit.

Key words. stars: abundances – stars: atmospheres – stars: Population II – globular clusters: general – globular clusters: individual: NGC 4833

1. Introduction

Globular clusters (GCs) are the brightest relics of the early phases of galaxy formation. Their study provides basic information on the early evolution of their host galaxy. In the past few years, it has become apparent that the episodes leading to the formation of these massive objects were complex. The main evidence for this complexity comes from the presence of chemical inhomogeneities that in most cases are limited to light elements involved in H-burning at high temperature (He, CNO, Na, Mg, Al), though in a few other GCs, star-to-star variations of heavier elements are also found (see reviews by Gratton et al. 2004, 2012). The extensive spectroscopic survey we are conducting (see e.g. Carretta et al. 2009a,b) revealed that these inhomogeneities are ubiquitous among GCs, but their range changes from cluster to cluster, being driven mainly by the total mass of the GCs, though metallicity and possibly other parameters also play a role.

Similar results have been obtained by other authors, using both similar analysis methods (e.g. Ramirez & Cohen 2002, 2003; Marino et al. 2008; Johnson & Pilachowski 2012) and photometric ones (e.g. Milone et al. 2012, 2013, and references therein). This has led to a general scenario where GCs host multiple stellar populations, often considered to correspond to different generations, where the younger stars (second-generation stars) are formed mainly or even exclusively from the ejecta of older ones (first or primordial generation stars: see e.g. D'Ercole et al. 2008; Decressin et al. 2008), though alternatives are also being considered (see e.g. Bastian et al. 2013a).

There are several key aspects that still require understanding. It is important to establish which of the first-generation stars polluted the material from which second-generation stars formed. This is relevant to setting both the involved time scale and the mass budget. Given that no variation in Fe abundance is observed in most GCs (see e.g. Carretta et al. 2009c), supernovae should play at most a very minor role, apart from a few exceptional cases. This clearly makes the chemical evolution of

⋆ Based on observations collected at ESO telescopes under programmes 083.D-0208 and 68.D-0265.

⋆⋆ Full Tables 2, 6–11 are only available at the CDS via anonymous ftp to cdsarc.u-strasbg.fr (130.79.128.5) or via http://cdsarc.u-strasbg.fr/viz-bin/qcat?J/A+A/564/A60

GCs very different from the one typically observed in galaxies, and requires a restriction of the mass range of the polluters. Several candidates have been proposed: the most massive among intermediate-mass stars during the asymptotic giant branch (AGB) phase (Ventura et al. 2001); fast-rotating massive stars (Decressin et al. 2007); massive binaries (de Mink et al. 2009); novae (Maccarone & Zurek 2012).

Arguments for or against each of these candidates exist, and it is not even clear if they should be considered as mutually exclusive. Scenarios based on different polluters produce different expectations about some observables (e.g. Valcarce and Catelan 2011). For instance, those involving massive stars are characterized by a very short time scale, which is possibly supported by the lack of evidence for multiple generation of stars in present-day massive clusters (Bastian et al. 2013b), though it is not very clear that such objects are as massive as the Milky Way GCs were when they formed. On the other hand, they have difficulty producing a well-defined threshold in cluster mass for the phenomenon (see Carretta et al. 2010a), as well as clearly separated stellar populations, as observed in several typical clusters from both photometry and spectroscopy (NGC 2808: D'Antona et al. 2005; Carretta et al. 2006, 2009a,b, 2012a,b; Piotto et al. 2007; M 4: Marino et al. 2008; NGC 6752: Milone et al. 2013; 47 Tuc: Milone et al. 2012, to quote a few examples).

Providing high quality data on more GCs is clearly needed to strengthen the results obtained so far. Spectroscopic analysis of rather large samples of stars may, for instance, be used to show whether stars can be divided into discrete groups in chemical composition, which may be explained more easily as evidence of multiple episodes of star formation, or rather distribute continuously. Also, very stringent limits on star-to-star variations in Fe abundances as observed in many GCs by Carretta et al. (2009c) or Yong et al. (2013) severely limit the possibility that SNe contributed to chemical evolution, which is one of the basic problems to be faced by short-timescale scenarios of cluster formation.

Following our earlier work (e.g. Carretta et al. 2006, 2009a,b), we present here the results of the analysis of large samples of spectra in NGC 4833, focussing on the Na-O anticorrelation, but also providing data for Fe, Mg, Al, Si, Ca, Ti, and other elements. This is the first extensive analysis of high dispersion spectra for this cluster since only two red giant branch (RGB) stars were analysed by Gratton and Ortolani (1989) and one by Minniti et al. (1996), which of course prevented any discussion on chemical inhomogeneities. NGC 4833 ($M_V = -8.16$: Harris 1996) has been classified as an old halo cluster with a moderately extended blue horizontal branch (Mackey & van den Bergh 2005) or an inner halo cluster (Carretta et al. 2010a). Studies of variable stars have been presented by Murphy & Darragh (2012, 2013), who found 17 RR Lyrae and six SX Phoenicis stars. The mean period of the RR Lyrae allows classifying the cluster as Oosterhoff II. NGC 4833 is seen projected close to the Coal Sack, and has a moderately large reddening ($E(B-V) = 0.32$) with non-negligible variations across the cluster. Casetti-Dinescu et al. (2007) determined a very eccentric orbit ($e = 0.84$) that brings the cluster very close to the Galactic center and never far from the Galactic plane ($z_{\rm max} = 1.8$ kpc, $r_a = 7.7$ kpc, $r_{\rm p} = 0.7$ kpc). Orbital parameters are similar to those of NGC 5986, so that a tentative association between the two clusters was proposed by Casetti-Dinescu et al.

The structure of this paper is as follows. Observations, radial velocities, and kinematics are presented in Sect. 2, while Sect. 3 is devoted to the abundance analysis, whose results are illustrated in Sect. 4. Our findings are discussed in Sect. 5 and summarised in Sect. 6.

2. Observations

The photometric catalogue for NGC 4833 is based on *UBVI* data (ESO programme 68.D-0265, PI Ortolani), collected at the Wide-Field Imager at the 2.2-m ESO-MPI telescope on 17–21 February 2002. The WFI covers a total field of view of $34' \times 33'$, consisting of 8, 2048×4096 EEV-CCDs with a pixel size of $0\farcs238$. The collected images were dithered to cover the gaps between the CCDs, and the exposure times were divided into shallow and deep so as not to saturate the bright red giant stars and, at the same time, sample the faint main sequence stars with a good signal-to-noise ratio (S/N).

The de-biasing and flat-fielding reduction of the CCD mosaic raw images employed the IRAF package MSCRED (Valdes 1998), while the stellar photometry was derived by using the DAOPHOT and ALLFRAME programs (Stetson 1994). For specific details of the photometric reduction process see Momany et al. (2004).

The absolute photometric calibration primarily employed the use of *UBVI* standard stars from Landolt (1992), as well as secondary stars from the Stetson library[1], which provides more numerous and relatively fainter *BVI* standards. The uncertainties in the absolute flux calibration were of the order of 0.06, 0.03, 0.03, and 0.04 mag for *UBVI*, respectively. The NGC 4833 catalogue was not corrected for sky concentration, caused by the spurious reflections of light and its subsequent redistribution in the focal plane (Manfroid et al. 2001). As a consequence, photometric comparisons to independent catalogues (based on a smaller field of view data) might reveal systematic offsets as a function of the distance from the centre of the WFI mosaic.

We selected a pool of stars lying near the RGB ridge line in the colour–magnitude diagram (CMD) and without close neighbours, i.e. without any star closer than 3 arcsec. (We also included cases with neighbours between 2 and 3 arcsec, but only if fainter by more than 2 mag.) The FPOSS tool was used to allocate the FLAMES (Pasquini et al. 2002) fibres.

The stars in our spectroscopic sample are indicated in Fig. 1. We clearly see that NGC 4833 is heavily contaminated by field stars of the Galactic disk and bulge, given its present location at $l = 303.60$ deg, $b = -8.02$ deg. Even if the reddening toward the cluster is high and differential (Melbourne & Guhathakurta 2004), thus complicating the analysis, the excision of non-members via radial velocity and the use of infrared filters for temperature determinations, as done in similar cases (see e.g. Gratton et al. 2006, 2007), make it feasible.

The log of the observations is given in Table 1. We obtained two exposures with the high resolution GIRAFFE grating and the setup HR11 covering the Na I 5682-88 Å doublet and two exposures with the setup HR13, including the [O I] forbidden lines at 6300–63 Å. Excluding a non-member star and another that was not useful owing to the low S/N of the spectrum, we observed a total of 12 (bright) giants with the fibres feeding the UVES spectrograph (Red Arm, with spectral range from 4800 to 6800 Å and $R = 47\,000$, indicated as blue squares in Fig. 1) and 73 with GIRAFFE (seven are in common). The median values of the S/N of spectra obtained with UVES and with the HR11 and HR13 setups of GIRAFFE are 90, 95, and 140, respectively.

We used the 1D, wavelength calibrated spectra as reduced by the ESO personnel with the dedicated FLAMES pipelines.

[1] http://cadcwww.hia.nrc.ca/standards/

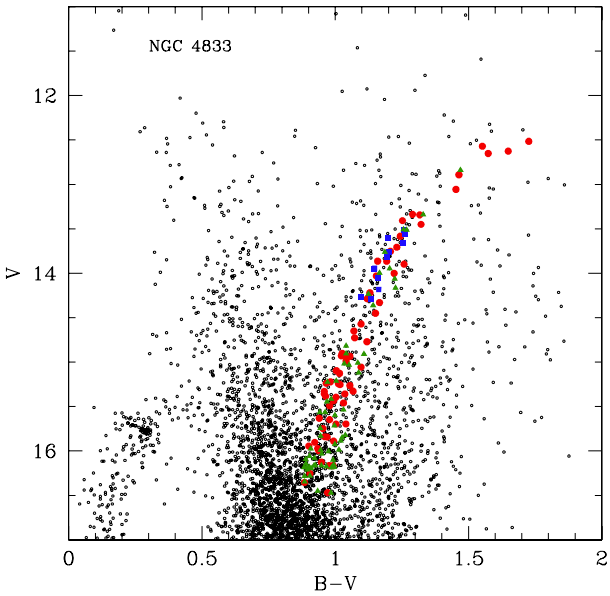

Fig. 1. $V, B-V$ CMD of NGC 4833 (open circles). Stars selected for the present study are plotted as filled, larger symbols: blue squares are the stars observed with UVES, red circles are stars with GIRAFFE spectra, and green triangles are stars observed with GIRAFFE but not analysed because found to be non-members from their RV (see text).

Table 1. Log of FLAMES observations for NGC 4833.

Date	UT	Exp. (s)	Grating	Seeing (″)	Airmass
Apr. 05, 2009	02:11:37.395	2700	HR11	1.07	1.599
Apr. 05, 2009	02:58:02.303	2700	HR11	1.09	1.519
Apr. 05, 2009	03:54:25.968	2700	HR13	0.64	1.462
Apr. 05, 2009	04:40:47.286	2700	HR13	0.59	1.446

Radial velocities (RV) for stars observed with the GIRAFFE spectrograph were obtained using the IRAF[2] task FXCORR, with appropriate templates, while those of the stars observed with UVES were derived with the IRAF task RVIDLINES.

The large RV of NGC 4833 makes it easy to isolate cluster stars from field interlopers. In Fig. 2 we show the histogram of the heliocentric RVs derived for all stars observed; the cluster is easily spotted as a narrow and isolated peak around $V_r \simeq 200$ km s^{-1}. We select the 78 stars with $180.0 \leq RV \leq 220$ km s^{-1} as candidate cluster members. Their membership is fully confirmed by the following chemical analysis, since they all have the same iron abundance, within the uncertainties. The nearest non-member in the velocity space has $RV = 141.6 \pm 0.7$ km s^{-1}, ~60 km s^{-1} apart from the systemic velocity of the cluster. A brief overview of the cluster kinematics is provided in Sect. 2.1.

Our optical B, V photometric data were integrated with K-band magnitudes from the Point Source Catalogue of 2MASS (Skrutskie et al. 2006) to derive atmospheric parameters as described below, in Sect. 3.

Coordinates, magnitudes, and heliocentric RVs are shown in Table 2 (the full table is only available at CDS).

[2] IRAF is distributed by the National Optical Astronomical Observatory, which is operated by the Association of Universities for Research in Astronomy, under contract with the National Science Foundation.

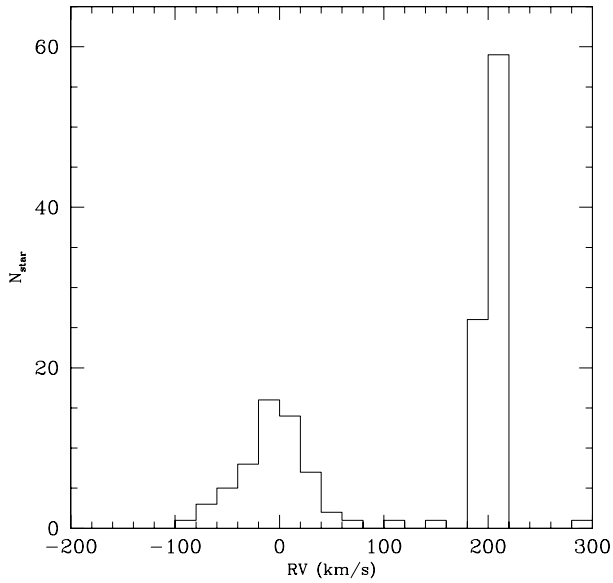

Fig. 2. Distribution of heliocentric radial velocities (RVs) for stars observed in NGC 4833.

2.1. Radial velocities and kinematics

There is no analysis in the literature dealing with the internal kinematics of NGC 4833, and no estimate of the central velocity dispersion σ_0. It is worth using our sample for a first investigation, although it is not especially well suited for this purpose. Indeed our 78 genuine cluster member stars are distributed (see Fig. 3) in the radial range $1.0 \leq R/r_c \leq 6.6$ or $0.4 \leq R/r_h \leq 2.8$[3]. We therefore cannot sample the kinematics in the cluster core and in the outer halo. (The tidal radius is $r_t = 17.8 r_c = 7.4 r_h$, since $c = 1.25$.) Our analysis is fully homogenous with the one in Bellazzini et al. (2012) for the other clusters included in our survey: for further details, we address the interested reader to that paper. The only difference is that here mean velocity and velocity dispersions are estimated with the maximum likelihood (ML) procedure described in Martin et al. (2007), which naturally takes the effect of errors on the individual RV measures into account.

First of all, we compared the RV estimates obtained from HR13 and HR11 spectra for the 45 stars that have valid RV measures from both setups. The mean difference for the 35 stars brighter than $V = 15.5$ (i.e. those with the smallest individual errors) is $\langle RV_{13} - RV_{11} \rangle = -0.43 \pm 0.07$ km s^{-1}. This shift was applied to the RV derived from HR11 spectra to bring all the RV estimates to a common zero point. Then, for each star, we adopted the RV estimated from HR13 spectra when present and when the individual uncertainty is lower than the HR11 estimate, and the RV from HR11 in the other cases.

Considering the whole sample of 78 stars, we find an average velocity of $\langle RV \rangle = 202.0 \pm 0.5$ km s^{-1} (and a dispersion of 4.1 ± 0.3 km s^{-1}), in very good agreement with the value reported by Harris (1996), $\langle RV \rangle = 200 \pm 1.2$ km s^{-1}. Fitting a King (1966) model with $c = 1.25$ to the velocity dispersion curve, we estimated the central velocity dispersion $\sigma_0 = 5.0 \pm 1.0$ km s^{-1}. We do not find any statistically significant rotation: in the notation of Bellazzini et al. (2012), the rotation amplitude is $A_{rot} = 0.9 \pm 0.5$ km s^{-1} and $A_{rot}/\sigma_0 = 0.18 \pm 0.11$.

[3] The values for the core radius r_c and the half-light radius r_h were taken, as all the cluster parameters that will be used in the following, from the 2010 version of the Harris (1996) catalogue.

Table 2. List and relevant information for target stars in NGC 4833.

ID	RA	Dec	B	V	K	RV(Hel)	Notes
22810	12 59 5.559	–70 56 59.87	16.470	15.491	12.337	198.79	HR11, HR13
23306	12 58 49.698	–70 55 17.19	16.736	15.696	12.439	205.33	HR11, HR13
23437	12 58 54.862	–70 54 59.07	16.153	15.056	11.711	195.26	HR11
23491	12 59 5.197	–70 54 53.86	14.242	12.516	8.270	200.33	HR11, HR13
23518	12 59 12.686	–70 54 50.03	16.395	15.359	12.206	203.73	HR13
24063	12 58 54.127	–70 53 46.86	14.660	13.343	9.651	203.13	HR13
24252	12 59 16.083	–70 53 28.91	14.916	13.663	10.046	202.26	UVES

Notes. The complete table is available at the CDS.

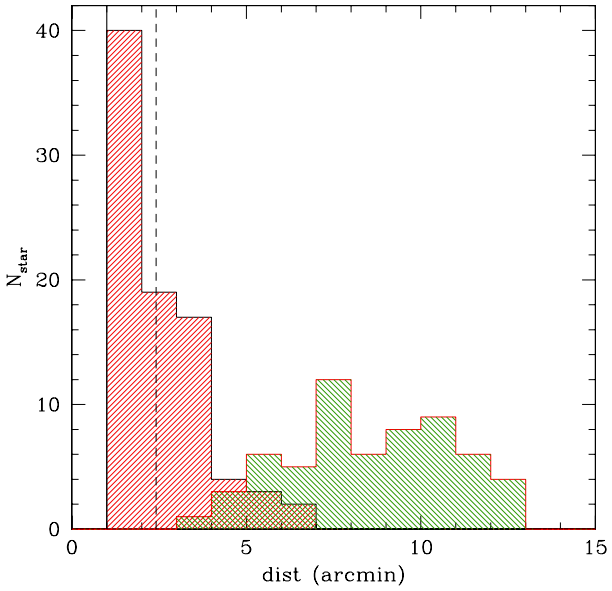

Fig. 3. Distribution of observed stars as a function of the radial distance from the centre of NGC 4833. Member stars are indicated in red, while green is used for non-members. The solid heavy line indicates the core radius (r_c = 1 arcmin), and the dashed line the half-mass radius (r_h = 2.41 arcmin) from Harris (1996).

As a result, NGC 4833 fits excellently into the correlations between metallicity (and horizontal branch morphology) and rotation found by Bellazzini et al.; i.e., metal-poor/blue HB clusters tend to have lower rotation than metal-rich/ red HB clusters.

Using the King (1966) formula, we estimate a dynamical mass $M_{\rm dyn} = 1.3^{+0.6}_{-0.5} \times 10^5\ M_\odot$, and $(M/L)_V = 0.84 \pm 0.45$, on the low side of the range covered by Galactic GCs (see Sollima et al. 2012; Pryor & Meylan 1993).

3. Abundance analysis

3.1. Atmospheric parameters

Following our tested procedure, effective temperatures $T_{\rm eff}$ for our targets were derived using an average relation between apparent magnitudes and first-pass temperatures from $V - K$ colours and the calibrations of Alonso et al. (1999, 2001). The rationale behind this adopted procedure is to decrease the star-to-star errors in abundances due to uncertainties in temperatures, since magnitudes are less affected by measure uncertainties than colours. In the case of NGC 4833, which is affected by high and variable reddening, we used the apparent K magnitudes in our relation with $T_{\rm eff}$ because the impact of the differential reddening on these magnitudes is very limited. This procedure worked very well on other GCs heavily affected by high and differential reddening patterns, such as the bulge clusters NGC 6441 (Gratton et al. 2006, 2007) and NGC 6388 (Carretta et al. 2007a). The adopted reddening $E(B - V) = 0.32$ mag is from the Harris (1996) catalogue, and it is in perfect agreement with the value derived in the accurate study by Melbourne et al. (2000), who provided an associated error of 0.03 mag. Using Table 3 of Cardelli et al. (1989), this translates into an error of 0.01 mag in K magnitudes that, in turn, corresponds to an uncertainty in temperature of 2.14 K, when coupled to the relation between effective temperature and K magnitude adopted for NGC 4833 in the present study.

Gravities were obtained from apparent magnitudes, assuming the $T_{\rm eff}$'s estimated above, bolometric corrections from Alonso et al. (1999), and the distance modulus for NGC 4833 from Harris (1996). We adopted a mass of 0.85 $M_\odot$ for all stars and $M_{\rm bol,\odot} = 4.75$ as the bolometric magnitude for the Sun, as in our previous studies.

We eliminated trends in the relation between abundances from Fe I lines and expected line strength (Magain 1984) to obtain values of the microturbulent velocity v_t.

Finally, using the above values we interpolated within the Kurucz (1993) grid of model atmospheres (with the option for overshooting on) to derive the final abundances, adopting the model with the appropriate atmospheric parameters for each star. Its abundances matched those derived from Fe I lines. As discussed in Carretta et al. (2013a), this choice has a minimal impact on the derived abundances with respect to models without overshooting.

3.2. Elemental abundances

Most of our derived abundances rest on the analysis of equivalent widths (EW). The code ROSA (Gratton 1988) was used, as in previous papers, to measure EWs by adopting a relationship between EW and FWHM, as described in detail in Bragaglia et al. (2001). Following the approach used in Carretta et al. (2007b), we first corrected the EWs from GIRAFFE spectra to the system of the higher resolution UVES spectra, using seven stars observed with both instruments. The correction has the form $EW_{\rm UVES} = 0.91(\pm0.02) \times EW_{\rm GIRAFFE} + 1.06(\pm0.49)$ with an rms scatter of 5.4 mÅ and a Pearson correlation coefficient of $r = 0.98$ from 121 lines.

Atomic parameters for the lines falling in the spectral range covered by UVES spectra and by setups HR11 and HR13 in the GIRAFFE spectra are comprehensively discussed in Gratton et al. (2003), together with the adopted solar reference abundances.

Before co-adding, each HR13 GIRAFFE spectrum was corrected for blending with telluric lines due in particular to H_2O and O_2 near the forbidden [O I] line at 6300 Å, using synthetic spectra as described in Carretta et al. (2006). Corrections for any effects of departures from the local thermodynamical equilibrium (LTE) assumption according to the descriptions by Gratton et al. (1999) were applied to the derived Na abundances.

We derived abundances of O, Na, Mg, and Si among the elements participating in the network of proton-capture reactions in H-burning at high temperature. Additionally, Al abundances were obtained from the doublet Al I 6696–98 Å for stars observed with UVES.

Besides Mg and Si (numbered among the proton-capture elements), we derived the abundance of the α-elements Ca and Ti I, and Ti was also obtained from the singly ionized species in stars with UVES spectra. Abundances for the Fe-peak elements Sc II, V I, Cr I, Cr II, Mn I, Ni I, and Zn I were also derived, with abundances of some species only obtained for stars with UVES spectra, because of the larger spectral coverage. Corrections due to the hyperfine structure (references in Gratton et al. 2003) were applied to Sc, V, Mn, and Co. Abundances of Cu I were derived from spectrum synthesis, as detailed in Carretta et al. (2011).

The concentration of the neutron-capture elements Y II, Ba II, La II, and Nd II was derived mostly for stars with UVES spectra and mostly from measurements of EWs. Results for Y and Ba were checked with synthetic spectra using line lists from D'Orazi et al. (2013) and D'Orazi et al. (2012), respectively. Abundances derived with the two methods are in very good agreement. Lanthanum abundances were obtained from EWs of three to four lines with transition parameters from Sneden et al. (2003; see also Carretta et al. 2011).

The available Ba lines are all very strong and quite sensitive to the velocity fields in the stellar atmospheres. As a consequence, a clear trend of Ba abundances as a function of the microturbulence results when using the values of v_t derived using the weaker Fe lines, formed typically in deeper atmospheric layers (see e.g. Carretta et al. 2013b, for a discussion of a similar effect in the analysis of NGC 362). To alleviate this problem, good results are obtained by adopting the values of v_t from the relation as a function of the surface gravity provided by Worley et al. (2013) for giants in the metal-poor GC M 15. When analysed using these values and a constant metallicity equal to the metal abundance derived for NGC 4833 (see next section), no trend is apparent, and we can safely explore the Ba abundances looking for intrinsic dispersion or correlations (if any) with other elements. The relation from Worley et al. was chosen since it was shown to efficiently remove any trend between Ba abundances and v_t for bright stars in a GC with metallicity comparable to NGC 4833. On average, the values of v_t from this relation are 0.26 km s^{-1} higher than the values derived as described in the previous section for individual stars (with rms = 0.29 km s^{-1}, 78 stars). However, for all other species, the last method works very well, and we adopted, for all elements except Ba, this approach that guarantees homogeneity with the more than 20 GCs analysed by our group in this FLAMES survey.

3.3. Metal abundances

The mean metallicity we found for NGC 4833 from stars with high resolution UVES spectra is [Fe/H]= −2.015 ± 0.004 ± 0.084 dex (rms = 0.014 dex, 12 stars) from neutral species, where the first error is from statistics and the second refers to the systematic effects, as estimated in the next section. From the large sample of stars with GIRAFFE spectra, we derived a value of [Fe/H]= −2.040 ± 0.003 ± 0.073 dex (rms = 0.024 dex, 73 stars).

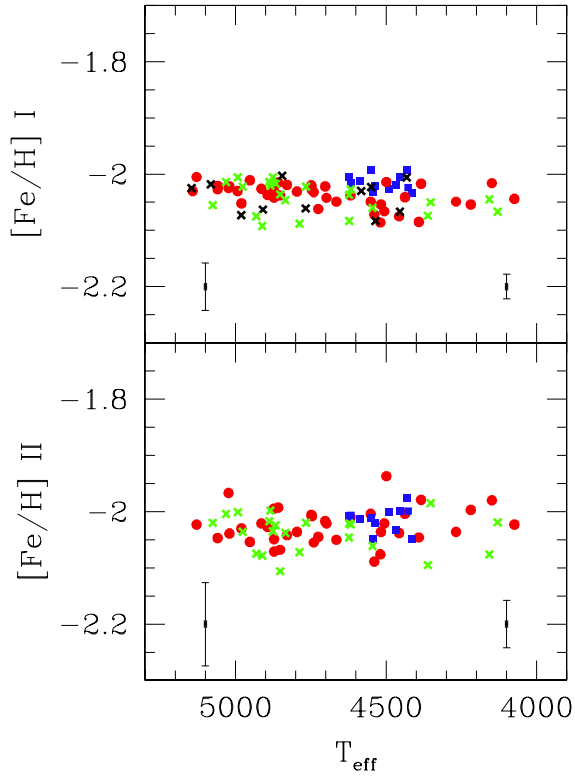

Fig. 4. Abundance ratios [Fe/H] I (*upper panel*) and [Fe/H] II (*lower panel*) as a function of T_{eff} for all analysed stars. Blue squares are stars with UVES spectra, filled circles are those with GIRAFFE spectra observed with both the HR11 and HR13 setups, and crosses indicate stars observed with only the HR11 (black) or the HR13 (green) setup. Error bars on the right and on the left are star-to-star errors for targets observed with UVES and GIRAFFE, respectively.

The abundances of iron obtained from the singly ionized species are in excellent agreement with those from neutral lines: [Fe/H]II = −2.014 (rms = 0.021 dex, 12 stars) from UVES and [Fe/H]II = −2.030 (rms = 0.033 dex, 59 stars) from GIRAFFE. The derived Fe abundances do not present any trend as a function of the effective temperature, as shown in Fig. 4.

Our average metal abundance seems to be about 0.2–0.3 dex lower than most of previous estimates in literature. From a preliminary analysis of RR Lyrae variables, Murray & Darragh (2013) find [Fe/H] = −1.67 ± 0.13 dex using Fourier decomposition of the light curves. We note, however, that the metallicities based on this method are often higher than those derived from high resolution spectroscopy, in particular in the low metallicity regime. For example, [Fe/H] = −1.98 dex from RR Lyrae in M 15 (Garcia Lugo et al. 2007), compared to [Fe/H] = −2.32 dex from high resolution spectroscopy (Carretta et al. 2009c); [Fe/H] = −1.23 dex for M 5 from RR Lyrae (Kaluzny et al. 2000) compared to −1.34 (Carretta et al. 2009c); [Fe/H] = −2.11 dex from variables in M 30 (Kains et al. 2013), and −2.34 from Carretta et al. (2009c). The discrepancy is not limited to our group and analysis: Figuera Jaimes et al. (2013) derived [Fe/H] = −1.64 from RR Lyraes in NGC 7492, while Cohen & Melendez (2005) found −1.82 dex for this cluster from high resolution spectra. Using high resolution spectra and the MARCS models, Kraft and Ivans (2003) find [Fe/H] = −2.33 dex and [Fe/H] = −2.39 dex for the metal-poor GCs M 30 and M 15, respectively.

Table 3. Sensitivities of abundance ratios to variations in the atmospheric parameters, to errors in the equivalent widths (EWs), and errors in abundances for stars of NGC 4833 observed with UVES.

Element	Average *n*. lines	$T_{\rm eff}$ (K)	log g (dex)	[A/H] (dex)	$v_{\rm t}$ km s^{-1}	*EW*s (dex)	Total internal	Total systematic
Variation		50	0.20	0.10	0.10			
internal		4	0.04	0.01	0.10	0.01		
systematic		57	0.06	0.08	0.03			
[Fe/H]I	39	+0.073	−0.016	−0.015	−0.016	0.014	0.022	0.084
[Fe/H]II	5	−0.017	+0.079	+0.018	−0.005	0.038	0.042	0.032
[O/Fe]I	1	−0.050	+0.091	+0.039	+0.014	0.085	0.088	0.090
[Na/Fe]I	2	−0.038	−0.030	−0.003	+0.011	0.060	0.061	0.096
[Mg/Fe]I	1	−0.029	+0.000	+0.002	+0.011	0.085	0.086	0.072
[Al/Fe]I	1	−0.034	+0.002	+0.003	+0.013	0.085	0.086	0.105
[Si/Fe]I	4	−0.050	+0.025	+0.011	+0.013	0.043	0.045	0.059
[Ca/Fe]I	15	−0.016	−0.006	−0.003	+0.003	0.022	0.022	0.018
[Sc/Fe]II	6	+0.011	−0.007	+0.003	+0.011	0.035	0.035	0.029
[Ti/Fe]I	5	+0.019	−0.005	−0.002	−0.014	0.038	0.040	0.014
[Ti/Fe]II	9	+0.025	−0.013	−0.002	−0.002	0.028	0.032	0.023
[V/Fe]I	2	+0.016	−0.006	−0.002	+0.013	0.060	0.062	0.019
[Cr/Fe]I	9	+0.013	−0.011	−0.007	−0.009	0.028	0.030	0.017
[Cr/Fe]II	4	−0.001	−0.011	−0.009	+0.000	0.043	0.043	0.013
[Mn/Fe]I	2	−0.012	−0.000	+0.001	+0.014	0.060	0.062	0.015
[Co/Fe]I	1	−0.014	+0.001	+0.003	+0.013	0.085	0.086	0.020
[Ni/Fe]I	8	+0.005	+0.008	+0.003	+0.007	0.030	0.031	0.007
[Cu/Fe]I	1	+0.010	+0.003	+0.001	+0.010	0.085	0.086	0.021
[Zn/Fe]I	1	−0.075	+0.056	+0.022	−0.001	0.085	0.085	0.088
[Y/Fe]II	9	+0.031	−0.012	+0.000	−0.013	0.028	0.031	0.040
[Ba/Fe]II	3	+0.043	−0.010	+0.002	−0.075	0.049	0.090	0.065
[La/Fe]II	3	+0.040	−0.009	+0.003	+0.001	0.049	0.049	0.046
[Nd/Fe]II	4	+0.041	−0.009	+0.003	−0.000	0.043	0.043	0.048

From CCD photometry, Melbourne et al. (2000) derived a mean metallicity [Fe/H] = −1.83 ± 0.14 dex (and a reddening $E(B-V)$ = 0.32 ± 0.03). Early detections based on high resolution spectra also obtained similar high values: [Fe/H] = −1.71 dex from one star (Minniti et al. 1996) and [Fe/H] = −1.74 dex, on average, from two stars (Gratton & Ortolani 1989). Moreover, Kraft and Ivans (2003) found for this GC a metallicity [Fe/H] = −2.06, −2.00, −2.04 dex from MARCS, and Kurucz models with and without the overshooting option, respectively.

3.4. Error budget

Our procedure for error estimates is amply described in Carretta et al. (2007b, 2009a,b) so will not be repeated here. In the following we only provide the main tables for the sensitivities of abundance ratios to the adopted errors in the atmospheric parameters and EWs and the final estimates of internal and systematic errors for all species analysed from the UVES and GIRAFFE spectra of stars in NGC 4833.

The sensitivities of derived abundances on the adopted atmospheric parameters were obtained by repeating our abundance analysis by changing only one atmospheric parameter each time for all stars in NGC 4833 (separately for the UVES and the GIRAFFE samples). The sensitivity in each parameter was adopted as the one corresponding to the average of all the sample.

The amount of the change in the input parameters $T_{\rm eff}$, log g, [A/H], and $v_{\rm t}$ to compute the sensitivity of abundances to variations in the atmospheric parameters is shown in the first line of the headers in Tables 3 and 4, whereas the resulting response in abundance changes of all elements (the sensitivities) are shown in columns from 3 to 6 of these tables.

The averages of all measured elements with their rms scatter are listed in Table 5. Derived atmospheric parameters and Fe abundances for individual stars in NGC 4833 are in Table 6; abundances of proton-capture, α-capture, Fe-peak, and neutron-capture elements are provided in Tables 7–11, respectively. These tables are only available at the CDS: a few lines are given for guidance. Upon request by the referee, we also report the average and rms scatter of the [Na/Fe] ratio in LTE for individual stars in the last two columns of Table 7, to give an idea of the adopted NLTE corrections.

4. Results

4.1. The Na-O anticorrelation in NGC 4833

After combining the UVES and GIRAFFE datasets and taking into account stars observed with both instruments, we ended with 61 stars with O abundances (40 actual detections and 21 upper limits) and 60 stars with Na abundances. The Na-O anticorrelation in NGC 4833 rests on 51 giants with both O and Na, and is shown in Fig. 5, with star-to-star errors relative to the GIRAFFE dataset. Internal error bars for the UVES sample are slightly smaller (see Table 3).

It is not easy to judge whether stars in NGC 4833 are grouped into discrete populations with homogeneous composition, along the Na-O anti-correlation, which is mostly formed with the stars observed with GIRAFFE. Similar large samples are better suited to quantifying the extension of this feature, but the associated internal errors may smear possible groups, although some subdivisions are recognizable in Fig. 5. The limited sample of giants observed with UVES seems to be better suited to this task.

The 12 stars with UVES spectra are clearly clustered in two clearly separated groups: one with abundances typical of the pattern established by core-collapse supernovae nucleosynthesis

Table 4. Sensitivities of abundance ratios to variations in the atmospheric parameters, to errors in the EWs, and errors in abundances for stars of NGC 4833 observed with GIRAFFE.

Element	Average n. lines	$T_{\rm eff}$ (K)	$\log g$ (dex)	[A/H] (dex)	$v_{\rm t}$ km s^{-1}	EWs (dex)	Total internal	Total systematic
Variation		50	0.20	0.10	0.10			
internal		4	0.04	0.02	0.22	0.02		
systematic		57	0.06	0.07	0.03			
[Fe/H]I	20	+0.064	−0.011	−0.011	−0.016	0.023	0.042	0.073
[Fe/H]II	2	−0.016	+0.077	+0.011	−0.004	0.071	0.074	0.030
[O/Fe]I	1	−0.040	+0.085	+0.031	+0.018	0.101	0.110	0.066
[Na/Fe]I	2	−0.034	−0.026	+0.004	+0.013	0.071	0.077	0.055
[Mg/Fe]I	1	−0.027	+0.001	+0.002	+0.013	0.101	0.105	0.039
[Si/Fe]I	3	−0.046	+0.021	+0.009	+0.015	0.058	0.067	0.053
[Ca/Fe]I	4	−0.015	−0.006	−0.001	+0.001	0.051	0.051	0.017
[Sc/Fe]II	4	−0.052	+0.082	+0.026	+0.011	0.051	0.059	0.064
[Ti/Fe]I	3	+0.004	−0.004	+0.001	+0.015	0.058	0.067	0.007
[V/Fe]I	3	+0.021	−0.008	−0.003	+0.020	0.058	0.073	0.025
[Cr/Fe]I	1	+0.011	−0.006	−0.001	+0.021	0.101	0.111	0.018
[Co/Fe]I	1	−0.001	+0.003	+0.005	+0.023	0.101	0.113	0.015
[Ni/Fe]I	3	−0.001	+0.008	+0.004	+0.013	0.058	0.065	0.006
[Ba/Fe]II	1	−0.033	+0.077	+0.024	−0.067	0.101	0.179	0.056

Table 5. Mean abundances from UVES and GIRAFFE.

Element	UVES			GIRAFFE		
	n	avg	rms	n	avg	rms
[O/Fe]I	12	+0.17	0.22	51	+0.25	0.29
[Na/Fe]I	12	+0.52	0.29	52	+0.46	0.27
[Mg/Fe]I	12	+0.27	0.22	44	+0.36	0.15
[Al/Fe]I	12	+0.90	0.34			
[Si/Fe]I	12	+0.47	0.04	66	+0.46	0.05
[Ca/Fe]I	12	+0.35	0.01	73	+0.35	0.02
[Sc/Fe]II	12	−0.04	0.01	73	−0.04	0.02
[Ti/Fe]I	12	+0.18	0.02	53	+0.17	0.02
[Ti/Fe]II	12	+0.23	0.01			
[V/Fe]I	12	−0.08	0.01	24	−0.10	0.02
[Cr/Fe]I	12	−0.24	0.02	24	−0.20	0.04
[Cr/Fe]II	12	+0.01	0.05			
[Mn/Fe]I	12	−0.54	0.01			
[Fe/H]I	12	−2.02	0.01	73	−2.04	0.02
[Fe/H]II	12	−2.01	0.02	59	−2.03	0.03
[Co/Fe]I	8	−0.03	0.03	7	−0.07	0.04
[Ni/Fe]I	12	−0.18	0.01	68	−0.18	0.03
[Cu/Fe]I	12	−0.80	0.09			
[Zn/Fe]I	12	+0.07	0.03			
[Y/Fe]II	12	−0.15	0.06			
[Ba/Fe]II	12	−0.06	0.07	62	−0.20	0.14
[La/Fe]II	12	+0.05	0.03			
[Nd/Fe]II	12	+0.42	0.04			

(high O and low Na), also shared by field stars of similar metallicity (e.g. Gratton et al. 2000), the other with low-O/high-Na abundances, whose counterparts are rarely observed in Galactic field stars. To check that this occurrence in NGC 4833 is not a spurious effect due to the limited number of giants in the UVES sample, we plotted in Fig. 6 (upper panel) the distribution of the [O/Na] ratios from our total sample of about 250 RGB stars observed with UVES in 22 GCs of the Milky Way in our FLAMES survey. The colour coding corresponds to the division of stars into the primordial (P) component of first generation stars, and to the two fractions of stars with intermediate (I) and extreme (E) composition within the second stellar generation in GCs, as defined in Carretta et al. (2009a) from their location along the Na-O anticorrelation. Our UVES sample in NGC 4833 (shown in Fig. 6 with number counts multiplied by a factor 3 to improve clarity) clearly splits into two groups, roughly coincident with the first and second generation stars. As a comparison, in the lower panel we also plot the only other large sample in an individual GC based on high resolution spectra, the about 100 RGB stars observed in M 4 by Marino et al. (2008). An offset of 0.1 dex was arbitrarily subtracted to their [O/Na] values to bring them on our abundance scale. In M 4, with its short anticorrelation, the extreme component of second-generation stars is obviously not present.

Using the quantitative criteria introduced by Carretta et al. (2009a), we can use O and Na abundances to quantify the fraction of the different stellar generations. From the total sample of 51 stars with O and Na, we found that the fractions of P, I, and E stars for NGC 4833 are 31 ± 8%, 59 ± 11%, and 10 ± 4%, respectively. The fraction of first-generation stars is similar to the one (about one third) typical of the overwhelming majority of Galactic GCs. On the other hand, the fraction of second-generation E stars with extremely modified composition is quite large in NGC 4833. As a comparison, the E fraction in GCs like NGC 4590 (M 68), NGC 6809 (M 55), NGC 7078 (M 15), NGC 7099 (M 30), bracketing NGC 4833 in mass and metallicity, does not exceed 2% or 3% (and it is formally absent in M 15 and M 68, Carretta et al. 2009a,b). Among the observed RGB stars in NGC 4833, there is apparently no statistically significant segregation in radial distance from the cluster centre for the P, I, and E components. Our sample of member stars is, however, all confined within two half-mass radii and may not be the optimal sample for this kind of analysis. Large photometric databases are better suited to studying possible difference of radial concentration of different stellar generations.

The interquartile range (IQR) for the ratio [O/Na] is a very useful measurement to quantify the extension of the Na-O anticorrelation (Carretta 2006). From our large sample we found that IQR[O/Na] = 0.945 dex in NGC 4833. Therefore, this cluster joins the ensemble of other GCs producing a nice correlation with the cluster total mass (represented by the proxy of the total absolute magnitude, $M_V = -8.16$ for NGC 4833 from Harris 1996), established in Carretta et al. (2010a) and reproduced in the left-hand panel of Fig. 7. The location of NGC 4833 in this plot seems to be in the upper envelope of the relation defined by

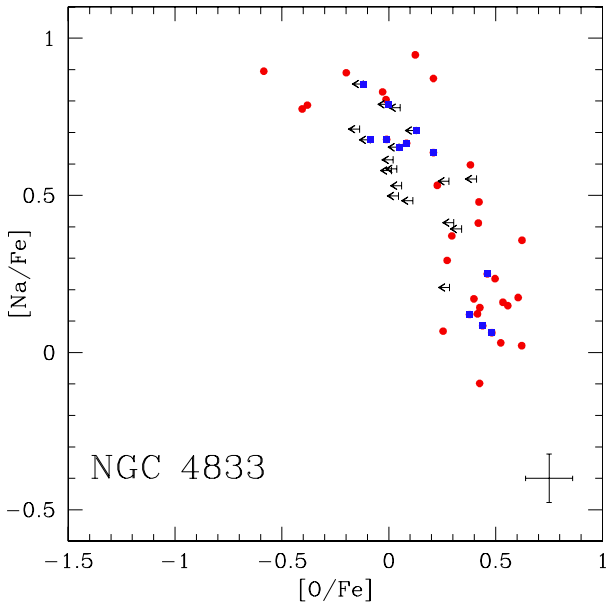

Fig. 5. Na-O anti-correlation observed in NGC 4833. Blue squares are stars observed with UVES, while red circles indicate stars with GIRAFFE spectra. Upper limits in O are shown as arrows, and star-to-star (internal) error bars are plotted.

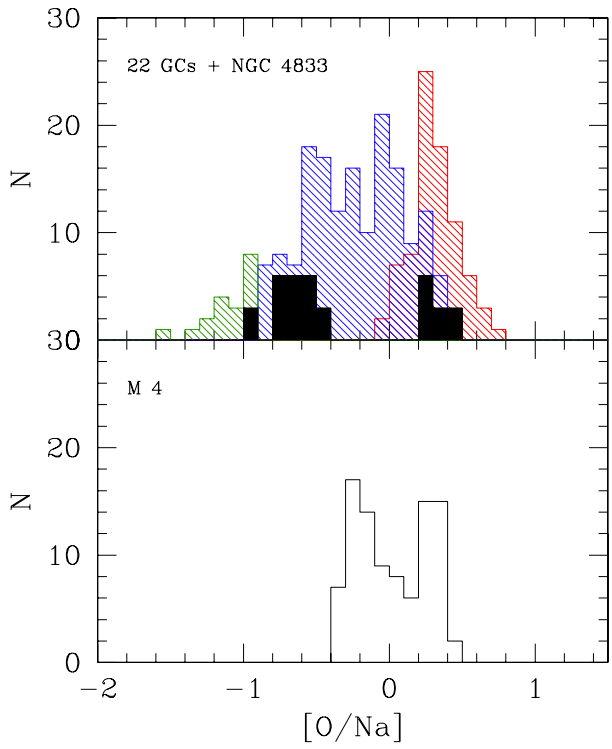

Fig. 6. Distribution of the [O/Na] abundance ratios in several GCs from stars observed with the high resolution UVES spectrograph. In the upper panel, about 250 RGB stars in 23 GCs from our FLAMES survey are plotted. Colour coding is red, blue, and green for the P, I, and E components defined in Carretta et al. (2009a). In black we plotted the distribution for NGC 4833 from the present work, with the numbers of stars multiplied by 3 to improve the visibility. *Lower panel*: distribution of [O/Na] from UVES spectra of about 100 giants in M 4 from Marino et al. (2008).

the bulk of the other GCs. The position of another cluster sharing a similar position (NGC 288) is also indicated. This occurrence is discussed in Sect. 5.

Recio-Blanco et al. (2006) computed the maximum temperature reached along the horizontal branch (HB) in NGC 4833: $\log T_{\rm eff} = 4.301$. The correlation between this parameter and the extension of the Na-O anticorrelation, discovered by Carretta et al. (2007c), is updated and shown in the right-hand panel of Fig. 7. Once again, NGC 4833 seems to lie at the upper envelope of the relation.

4.2. Other proton-capture elements

Apart from the case of O and Na, significant star-to-star abundance variations are detected for other proton-capture elements in giants in NGC 4833. In particular, we found that the [Mg/Fe] abundance ratio shows an unusually wide spread in this cluster, with peak-to-peak variations of more than 0.5 dex.

The reality of the intrinsic scatter in Mg is immediately evident when comparing the estimated internal error for the UVES sample (0.086 dex) to the observed rms scatter in [Mg/Fe] (0.223 dex): the cosmic spread in Mg among RGB stars in NGC 4833 is significant at almost a 3σ level.

The run of [Mg/Fe] ratios as a function of the abundance of the proton-capture elements O, Na, and Si is shown in Fig. 8, together with the classical Na-O anticorrelation. The error bars indicate star-to-star errors and refer to the GIRAFFE sample; internal errors for stars in the UVES sample are usually smaller (see Table 3). The Mg abundance is correlated to that of O and anti-correlated with species enhanced in the network of proton-capture reactions, namely Na and Si. We retrieved this pattern from both the datasets observed with UVES and with GIRAFFE.

In the case of the GIRAFFE sample, the observed spread in Mg (0.151 dex) does not formally exceed the associated internal error (0.105 dex) too much, most likely thanks to the lower resolution of the spectra and the extension of the GIRAFFE sample to warmer giants, with weaker lines. However, even in this case there is no doubt that Mg variations in NGC 4833 are real. In Fig. 9 the HR11 spectra of the two stars with the lowest Mg abundances in the GIRAFFE sample (star 36391, with [Mg/Fe] = + 0.02 dex, and star 34613 with [Mg/Fe] = 0.00) are compared to the spectra of two other stars with similar

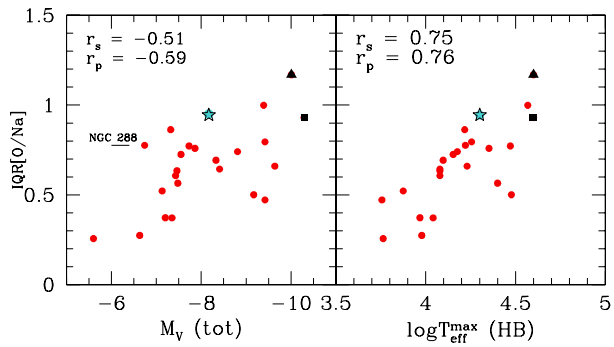

Fig. 7. IQR[O/Na] ratios for NGC 4833 (star symbol) and other Galactic GCs as a function of the total cluster absolute magnitude M_V (*left panel*). The other clusters are ω Cen (filled square, Johnson and Pilachowski 2010), M 54 (filled triangle, Carretta et al. 2010b), and other GCs from our FLAMES survey (filled circles, Carretta et al. 2009a, 2011, 2013b). In *the right panel* the IQR[O/Na] is shown as a function of the maximum temperature on the horizontal branch, from Recio-Blanco et al. (2006). In each panel, the Spearman rank correlation coefficient (r_s) and the Pearson's correlation coefficient (r_p) are reported.

Table 6. Adopted atmospheric parameters and derived iron abundances.

Star	$T_{\rm eff}$ (K)	log g (dex)	[A/H] (dex)	$v_{\rm t}$ (km s^{-1})	nr	[Fe/H]I (dex)	rms	nr	[Fe/HII (dex)	rms
22810	4893	2.17	−2.04	1.46	23	−2.037	0.118	2	−2.027	0.115
23306	4914	2.20	−2.03	1.44	21	−2.026	0.140	1	−2.021	
23437	4767	1.89	−2.06	1.19	5	−2.061	0.062			
23491	4074	0.45	−2.04	2.07	38	−2.044	0.105	3	−2.023	0.037
23518	4867	2.12	−2.02	1.43	20	−2.017	0.101	2	−2.024	0.001
24063	4352	1.04	−2.05	1.88	26	−2.050	0.090	2	−1.985	0.005
24252	4432	1.20	−1.99	1.88	38	−1.992	0.058	5	−1.975	0.040

Notes. The complete table is available is at the CDS.

Table 7. Abundances of proton-capture elements in stars of NGC 4833.

Star	n	[O/Fe]	rms	n	[Na/Fe]	rms	n	[Mg/Fe]	rms	n	[Al/Fe]	rms	limO	limAl	[Na/Fe]$_{\rm LTE}$	rms
22810	1	+0.23		3	+0.53	0.04	1	+0.34					1		+0.49	0.05
23306	1	+0.62		2	+0.36	0.10	2	+0.59	0.03				1		+0.28	0.11
23437				2	+0.36	0.03	1	+0.39					1		+0.22	0.03
23491	1	−0.01		3	+0.80	0.05	2	+0.25	0.02				1		+0.38	0.05
23518	1	+0.55					1	+0.47					1			
24063	2	−0.20	0.03	2	+0.89	0.00							1		+0.58	0.00
24252	1	+0.48		2	+0.06	0.02	1	+0.58		1	+0.43		1	0	−0.12	0.02

Notes. n is the number of lines used in the analysis. Upper limits (limO, Al = 0) and detections (=1) for O and Al are flagged. The complete table is at the CDS.

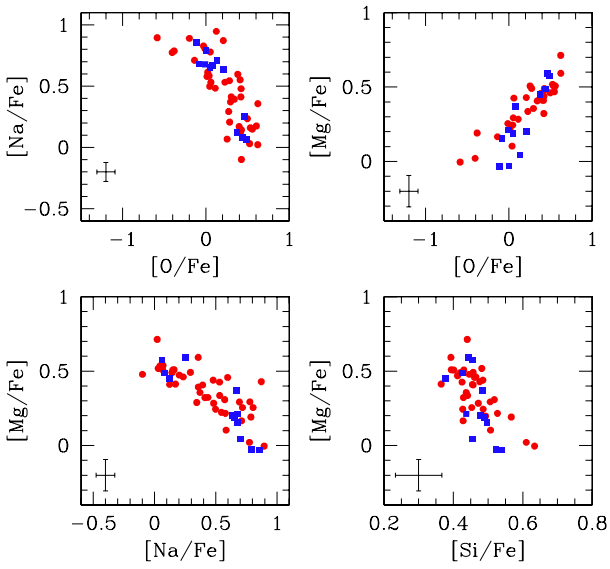

Fig. 8. Relations among proton-capture elements O, Na, Mg, and Si in NGC 4833. Red circles refer to stars with GIRAFFE spectra, blue squares indicate stars observed with UVES. The internal errorbars plotted in each panel are those relative to the GIRAFFE sample.

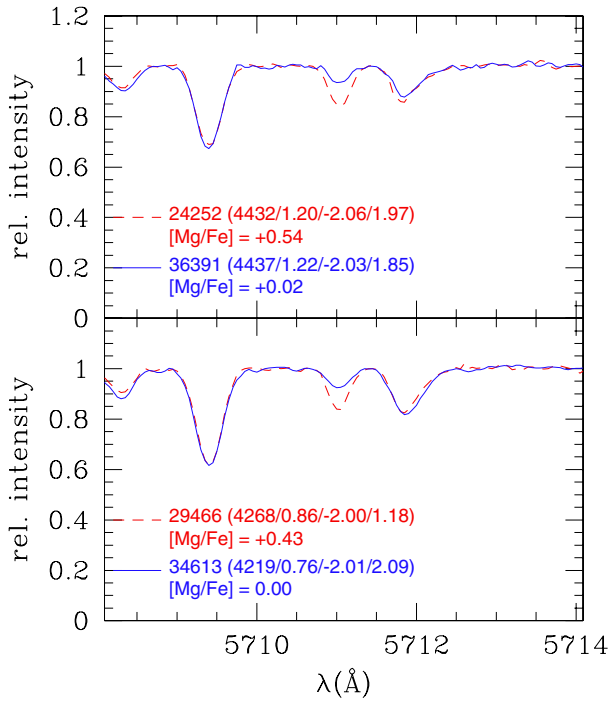

Fig. 9. Comparison of two pairs of Mg-poor and Mg-normal stars with similar atmospheric parameters in the Mg I 5711.09 Å spectral region. Atmospheric parameters $T_{\rm eff}$, log g, metallicity, $v_{\rm t}$, and the [Mg/Fe] abundance ratios of stars are indicated in each panel.

atmospheric parameters, but quite different (much higher) Mg abundances.

This direct comparison, free of any uncertainties related to the abundance analysis, robustly corroborates our findings: there is a wide spread in Mg in NGC 4833, where giants with a solar [Mg/Fe] ratio stand side-by-side with stars having a normal [Mg/Fe] ratio appropriate for metal-poor halo stars.

Large depletions of Mg due to the action of proton-capture reactions in H-burning at high temperature should have two main consequences: produce Al through the Mg-Al cycle and, if the burning temperatures are high enough, slightly enhance the abundance of Si through the mechanism of the leakage from the Mg-Al cycle on ^{28}Si (Karakas & Lattanzio 2003).

Abundances of Al can be obtained from the UVES spectra, but in four out of 12 stars observed with UVES only upper limits could be derived. Nevertheless, the derived values do not show any trend as a function of the effective temperature, and their

Table 8. Abundances of α-elements in stars of NGC 4833.

Star	n	[Si/Fe]	rms	n	[Ca/Fe]	rms	n	[Ti/Fe] I	rms	n	[Ti/Fe] II	rms
22810	6	+0.44	0.22	4	+0.36	0.05	1	+0.19				
23306	2	+0.39	0.01	6	+0.35	0.09	2	+0.17	0.09			
23437	2	+0.51	0.06	1	+0.31							
23491	6	+0.45	0.14	5	+0.34	0.12	4	+0.15	0.05			
23518	1	+0.41		3	+0.38	0.02	1	+0.17				
24063	1	+0.40		5	+0.37	0.05	3	+0.17	0.01			
24252	5	+0.45	0.06	13	+0.35	0.05	7	+0.17	0.06	8	+0.22	0.04

Notes. n is the number of lines used in the analysis. The complete table is at the CDS.

Table 9. Abundances of Fe-peak elements in stars of NGC 4833.

Star	n	[Sc/Fe] II	rms	n	[V/Fe]	rms	n	[Cr/Fe] I	rms	n	[Cr/Fe] II	rms	n	[Mn/Fe]	rms	n	[Co/Fe]	rms	n	[Ni/Fe]	rms	n	[Cu/Fe]	rms	n	[Zn/Fe] I	rms
22810	4	–0.04	0.09																3	–0.16	0.27						
23306	5	–0.03	0.24																2	–0.23	0.19						
23437	5	–0.06	0.06																2	–0.15	0.18						
23491	6	+0.00	0.04	4	–0.11	0.03	2	–0.21	0.10							1	–0.09		6	–0.16	0.11						
23518	1	–0.03																	2	–0.19	0.06						
24063	2	–0.05	0.08	2	–0.09	0.05	1	–0.20											3	–0.16	0.06						
24252	8	–0.05	0.14	4	–0.10	0.01	12	–0.21	0.07	6	+0.01	0.08	2	–0.54	0.08	1	–0.05		9	–0.17	0.07	1	–0.85		1	+0.04	

Notes. n is the number of lines used in the analysis. The complete table is at the CDS.

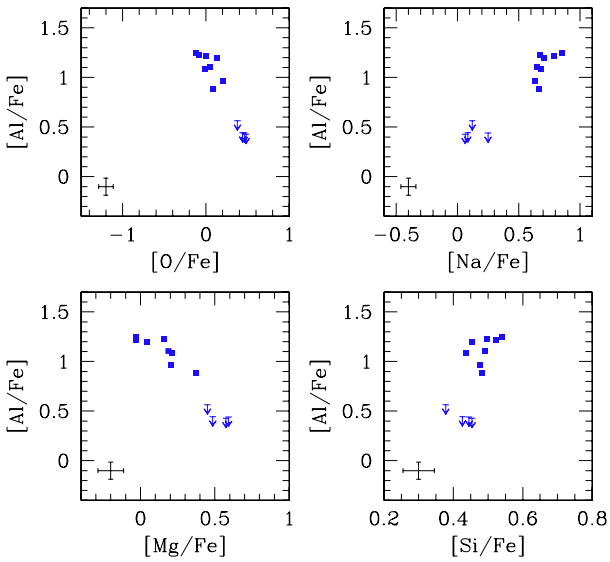

Fig. 10. Relations of Al with the proton-capture elements O, Na, Mg, and Si in giants of NGC 4833 observed with UVES spectra. Error bars represent internal errors associated to the UVES sample. The upper limits in Al abundances are indicated by arrows.

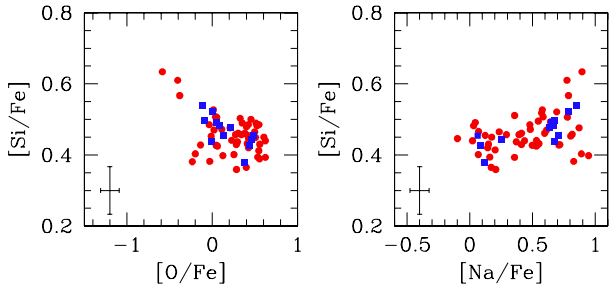

Fig. 11. Relations among proton-capture element ratios [Si/Fe], [O/Fe], and [Na/Fe] in NGC 4833. Blue squares indicate stars of the UVES sample, red circles are for stars observed with GIRAFFE. The internal error bars refer to the latter sample.

position instead reveals clear patterns (Fig. 10), with the typical correlations and anticorrelations among elements produced or destroyed, respectively, by the interplay of the Ne-Na and Mg-Al cycles (Denisenkov & Denisenkova 1989; Langer et al. 1993). Moreover, the sample, albeit limited, splits into two clearly separated groups.

The Mg-Si anticorrelation in Fig. 8, together with the Si-Al correlation (Fig. 10), already shows that some Si production occurred in the polluters of the first stellar generation in NGC 4833. To support this evidence further, we plot in Fig. 11 the [Si/Fe] ratios as a function of the O and Na values. The evidence of a Si-O anticorrelation is not robust for the GIRAFFE sample, but is clear for the more limited UVES sample. The correlation between Si and Na is represented in both samples well. The two stars with the lowest Mg abundances (Figs. 8 and 9) are also those showing the highest Si abundances, leaving no doubt that trends in Si and Mg are due to a common mechanism.

4.3. Other elements

The pattern of the α-elements measured in NGC 4833 is shown as a function of the effective temperatures for individual stars in Fig. 12, including also species like Mg and Si involved in the proton-capture reactions discussed in the previous section.

The vertical scale, bracketing the range of [Mg/Fe] ratios, is the same for all the elements to effectively show the large intrinsic dispersion of Mg and, partly, of Si with respect to other α-elements with no intrinsic scatter in NGC 4833.

The run of elements of the Fe-peak Sc, V, Cr, Co, and Ni as a function of the temperature is shown in Fig. 13 for individual stars in NGC 4833 from the UVES and GIRAFFE samples. These elements present no surprise; they track iron, as in most GCs, with no trend as a function of the $T_{\rm eff}$. The elements Mn and Cu, only available for stars with UVES spectra, show the underabundance typical of metal-poor GCs (e.g. Simmerer et al. 2003; Sobeck et al. 2006).

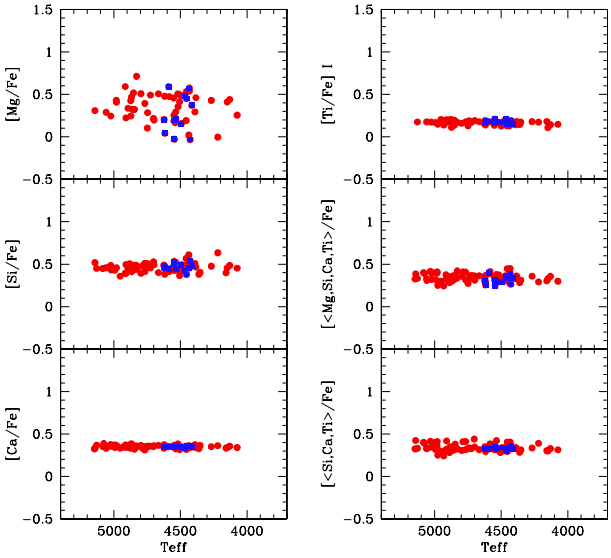

Fig. 12. Abundance ratios of α-elements Mg, Si, Ca, Ti I as a function of the effective temperature. The average of [α/Fe] ratios are shown in the last two panels on *the right column* (including and excluding the Mg abundance from the mean, respectively). Blue squares are UVES stars. Internal error bars are provided in Tables 3 and 4.

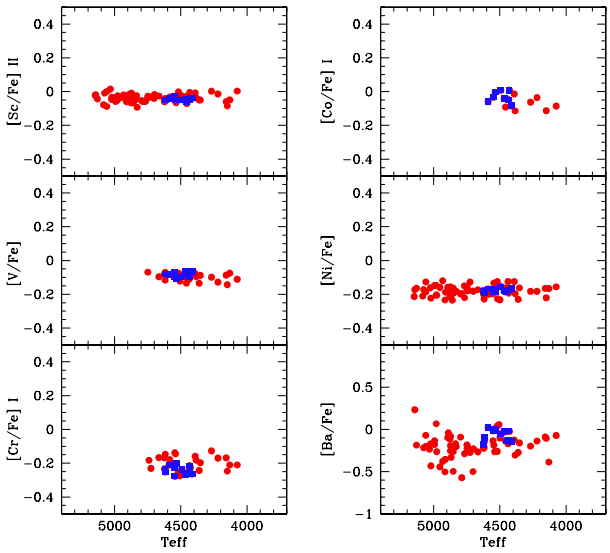

Fig. 13. Abundance ratios of elements of the Fe-peak (Sc II, V, Cr, Co, Ni) and of the neutron-capture element Ba as a function of the effective temperature. Blue squares are UVES stars. Note the different vertical scale for the panel with Ba abundances. Internal error bars are provided in Tables 3 and 4.

In the bottom right-hand panel of Fig. 13 we plot the abundance ratios of Ba, the only neutron-capture element available for a large sample of stars in NGC 4833. As explained in Sect. 3.2, our finally adopted Ba abundances, displayed in this panel, are those obtained by using for all stars a fixed model metal abundance ([Fe/H]= −2.02 dex, the average from the UVES spectra), and the microturbulence from the relation $v_t = 2.386 - 0.3067 \log g$ derived by Worley et al. (2013) for giants in the metal-poor GC M 15.

As recently shown in Worley et al. (2013) and Carretta et al. (2013a), this approach is quite effective in eliminating any trends of Ba abundances as a function of v_t and in reducing the ensuing spurious large scatters of the average. Only for Ba do we

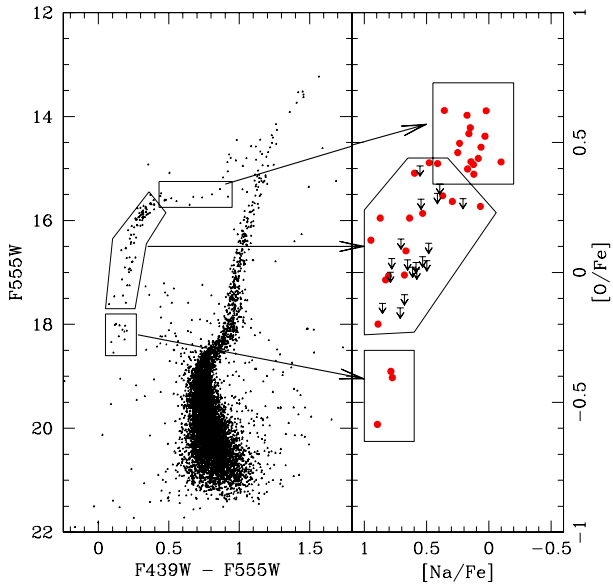

Fig. 14. HST colour–magnitude CMD of NGC 4833 from the snapshot survey by Piotto et al. (2002, *left*). The selected regions along the distribution of HB stars are tentatively associated to different groups along the Na-O anticorrelation from the present work (*right panel*).

then adopt these values, since our intent is simply to state that this neutron-capture element from the *s*-process in NGC 4833 (i) does not have an intrinsic dispersion (compare the rms scatters of the means in Table 5 with the internal errors in Tables 3 and 4); and (ii) there is no relation between Ba and elements involved in proton-capture reactions.

We cannot estimate the relative contribution of the *r*- and *s*-process of neutron capture from our data, because we did not measure a reliable abundance for the typical species that, like Eu, primarily sample an almost pure *r*-process nucleosynthesis at all metal abundances. For the [Ba/Y] ratio, we found an average value of 0.09 dex for NGC 4833 (rms = 0.06 dex, 12 stars), which is perfectly compatible with the ratios of field stars and GCs of similar metallicity (see e.g. Venn et al. 2004).

As for Ba, we found no correlation or anti-correlation whatsoever between the abundances of the *s*-process element La and the abundances of proton-capture elements.

5. Discussion

The Na-O anticorrelation among RGB stars in NGC 4833 reaches a quite long extension. This result must not come unexpected. A statistically robust relation between the extent of the Na-O anticorrelation and the hottest point along the HB is well known (Carretta et al. 2007c, 2010a). On the other hand, the HB in NGC 4833 presents a long blue tail, which stands out clearly, free of field contamination, in particular when high resolution HST imaging is used to construct the CMD (Fig. 14, left panel). Therefore, it would have been easy to predict a long Na-O anticorrelation in this cluster, which is exactly what we found with the current analysis.

It is tempting to associate the groups selected on the HB in the left-hand panel of Fig. 14 to the RGB stars distributed in the Na-O anticorrelation (right panel of the same figure). After all, RGB stars should end up on the HB after igniting He burning at the centre. Qualitatively, the tentative correspondences illustrated in Fig. 14 may work well, provided that no strong radial gradients are present between our spectroscopic sample and the

Table 10. Abundances of $n-$capture elements in stars of NGC 4833 with UVES spectra.

Star	n	[Y/Fe] II	rms	n	[La/Fe] II	rms	n	[Nd/Fe] II	rms
24081	10	−0.15	0.11	4	+0.30	0.16	4	+0.45	0.09
24252	6	−0.24	0.07	5	+0.35	0.12	4	+0.47	0.05
31163	10	−0.11	0.08	3	+0.25	0.07	4	+0.36	0.10
31332	10	−0.09	0.10	4	+0.40	0.13	4	+0.39	0.11
33347	9	−0.19	0.09	3	+0.30	0.04	4	+0.44	0.10
33554	10	−0.13	0.09	4	+0.25	0.15	4	+0.42	0.09
35680	5	−0.09	0.06	3	+0.35	0.06	4	+0.40	0.11
36402	7	−0.24	0.09	2	+0.25	0.22	3	+0.44	0.04
36454	9	−0.16	0.13	3	+0.25	0.11	3	+0.36	0.07
36484	9	−0.12	0.09	3	+0.40	0.06	4	+0.41	0.13
37197	9	−0.23	0.14	2	+0.50	0.05	3	+0.40	0.15
37498	9	−0.10	0.10	4	+0.25	0.07	4	+0.46	0.07

Notes. n is the number of lines used in the analysis. The complete table is at the CDS.

Table 11. Abundances of Ba II in stars of NGC 4833.

Star	N	[Ba/Fe] II	rms
22810	1	−0.10	
23306	1	−0.50	
23437			
23491	1	−0.07	
23518	1	−0.33	
24063	1	−0.16	
24252	3	−0.13	0.01

Notes. n is the number of lines used in the analysis. The complete table is at the CDS.

photometric sample, which cover different parts of the cluster. More quantitative relations must, of course, await spectroscopic abundance analysis of in situ HB stars.

However, the major peculiarity we uncovered in NGC 4833 is maybe the wide spread in Mg, whose abundance is clearly affected by large changes with respect to the usual plateau established by supernovae nucleosynthesis. As discussed in previous sections, we presented proofs that the Si abundance is partially modified by proton-capture reactions in this cluster also. This phenomenon was first observed by Yong et al. (2005) in NGC 6752, another metal-deficient GC with a long blue tail on the HB, and afterwards individuated through Si-Al correlations or Si-Mg anticorrelations in a number of other GCs (Carretta et al. 2009b). It is worth noting that in our large FLAMES survey, we found significant changes in the Mg (and Si) abundances only in massive and/or metal-poor GCs.

The leakage from the Mg-Al cycle on ^{28}Si puts a strong constraint on the temperature at which H-burning occurred in the stars responsible for polluting the intracluster gas, because the reaction producing ^{28}Si becomes dominant when $T_6 \sim 65$ K (Arnould et al. 1999, where the temperature is expressed in millions of Kelvin).

As a result, although this constraint does not allow the type of stars providing the raw material for the formation of the second- generation to be distinguished (see Prantzos et al. 2007, their Fig. 8), a logical question is whether NGC 4833 is another case like NGC 2419, although scaled down in amount of the involved elemental variations. In the distant halo cluster NGC 2419, the third most massive GC in our Galaxy Cohen and Kirby (2012) and Mucciarelli et al. (2012) discovered a double population of stars on the RGB. One group is made of Mg-normal giants with nearly solar abundance of potassium, whereas the other includes stars with a huge depletion of Mg (and large enhancement of K) that apparently do not have a counterpart in any of the other Galactic GCs observed so far concerning K abundances (Carretta et al. 2013b).

In the scenario of multiple populations in GCs, Ventura et al. (2012) claim that the pattern of abundances observed in NGC 2419 may be explained also by proton-capture reactions occurring in a much higher temperature range than usually observed in more normal cluster stars, which is favoured by the low metallicity of the cluster. In these particular cases, the production of Al from the destruction of Mg would be accompanied by the activation of synthesis of heavier elements, such as K, Ca, and also Sc by proton captures on Ar nuclei. The chief signature of this extreme burning would be the observation of anticorrelations between these elements and Mg, and in NGC 2419 we verified that the hypothesis by Ventura et al. agrees with observations (Carretta et al. 2013b).

NGC 4833 is far from being as massive as NGC 2419, however we observed a clear signature of processing in H-burning at very high temperature in its abundance pattern; moreover, it is a metal-poor cluster. We then checked the run of Si, Sc, and Ca as a function of Mg abundances in NGC 4833, but no anti-correlation was found, apart from the one between Si and Mg already discussed above. There is only a hint of a correlation between Ca and Sc, which can be intriguing, because formally such a correlation may be expected if both these elements are produced by burning Mg under the conditions invoked by Ventura et al. (2012). Unfortunately, the associated internal errors are large with respect to the amount of the variations, and the correlation is scarcely statistically significant. (The Pearson correlation coefficient is only 0.25; with a number of degrees of freedom exceeding 70 this implies that the correlation is significant only at about 95–98% in two-tail tests.)

Therefore, NGC 4833 cannot be considered a true sibling of NGC 2419, which continues to represent a unicum among GCs. Nevertheless, we find in the present study that NGC 4833, with its associated extreme chemistry, stands out among other globular clusters. To illustrate this finding we used the [Ca/Mg] vs. [Ca/H] plane adopted in Carretta et al. (2013b) as a diagnostic for the relevance of the high temperature nuclear cycles possibly activated in polluters of the first generation in GCs. While measurements of the K abundance are still scarce, Ca and Mg are measured for a large number of stars, providing the precious advantage of large statistics.

In Fig. 15 we updated this diagnostic plot by adding stars from NGC 4833 analysed in the present paper. Typically, the [Ca/Mg] ratios in GC stars show a narrow spread over a range of about 2 dex in Ca, with a few exceptions, represented by a few giants in ω Cen and M 54. These are the two most massive clusters in the Galaxy, considered to be the nuclei left from dwarf galaxies accreted in the past. The three Mg-poor stars in NGC 2808 (Carretta et al. 2009b) stand out around [Ca/H] ~ -0.85 dex, while in the low metallicity regime, the stars of NGC 4833 show a large dispersion in [Ca/Mg] when compared to other GCs. The spread in NGC 4833 does not reach the high values of the peculiar Mg-poor component in NGC 2419; however, the stars in NGC 4833 with the largest depletion in Mg reach the same level of the most Mg-poor stars in ω Cen. We caution the reader that among GCs stars, small offsets could exist with respect to the samples by Cohen & Kirby, Mucciarelli et al., and Norris & Da Costa, whereas all other RGB stars are from the homogeneous analysis by our group. There is no doubt that NGC 4833 shares some of the peculiarities also seen in ω Cen, M 54, and NGC 2808, although all these

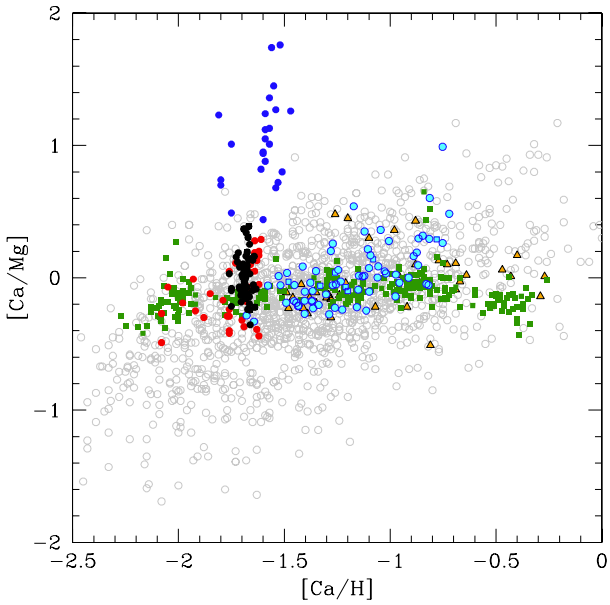

Fig. 15. [Ca/Mg] ratio as a function of the Ca abundances for several stellar populations, adapted from Carretta et al. (2013b). Grey open circles are stars in eight dwarf spheroidal Milky Way satellite galaxies (Kirby et al. 2011); blue and red filled circles are RGB stars in NGC 2419 with [Mg/Fe] lower and larger than 0.0 dex, respectively, from Cohen & Kirby (2012) and Mucciarelli et al. (2012). Orange triangles are giants in ω Cen (Norris & Da Costa 1995), cyan circles are RGB stars in M 54 (Carretta et al. 2010b). Green squares are for giants in 22 Galactic GCs (Carretta et al. 2009b, 2010c, 2011, 2013a,b). Black symbols are stars in NGC 4833 from the present study (squares and circles for the UVES and GIRAFFE samples, respectively).

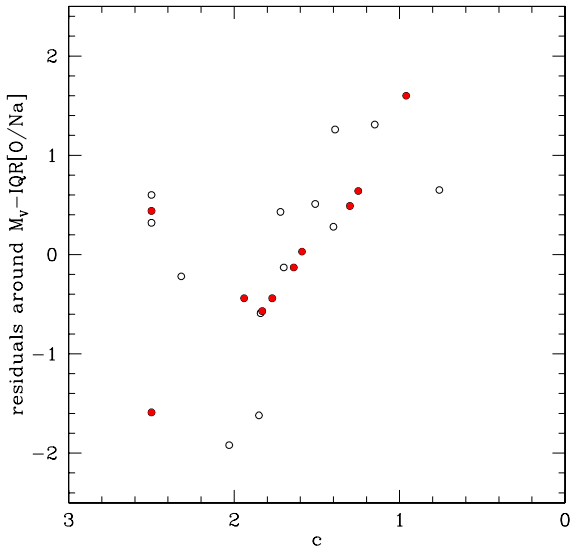

Fig. 16. Residuals around the relation between total absolute cluster magnitude M_V and the interquartile range IQR[O/Na] as a function of the cluster concentration c for GCs from our FLAMES survey. Filled points indicate inner halo clusters, as defined in Carretta et al. (2010a).

GCs are far from reaching the huge Mg-depletions observed in NGC 2419.

All these objects are high mass clusters, while the extension of the HB and of the Na-O anticorrelation (and, overall, of the proton-capture processing) are quite large in NGC 4833 with respect to its absolute magnitude. We could therefore wonder why NGC 4833 is not as massive.

In Fig. 7 we indicated the position of NGC 288 in the relation between the extension of the Na-O anticorrelation and total cluster mass (luminosity). In Carretta et al. (2010a), we discussed the evidence that GCs lying left of this relation lost a larger-than-average fraction of their mass after their formation. This conclusion stemmed from old, classical proofs (such as tidal tails associated to NGC 288, Leon et al. 2000) or from a new interpretation of independent observations (e.g. the number density of X-ray sources in M 71, see Sect. 5.3 in Carretta et al. 2010a).

Is there any indication of a huge mass loss also in NGC 4833? The field of view around NGC 4833 is very crowded (see Fig. 1), with variable reddening, and this probably deterred investigations looking for tidal tails around GCs, because we are not aware of any studies of this kind for NGC 4833.

Another approach could be to look for clues from the present-day mass function (PDMF). Unfortunately, there seems to be no determination of the PDMF for NGC 4833, again probably bacause of the difficulties related to the above-mentioned conditions. We note that GCs with central brightness μ_V, concentration, and central density ρ_0 similar to those of NGC 4833 present a PDMF with a rather steep slope of about –1 (de Marchi & Pulone 2007; Paust et al. 2010), indicating many low mass stars, and therefore little evidence of mass loss.

However, these other GCs are characterised by less critical orbits. Dynamical considerations suggest that NGC 4833 could actually be in a phase of destruction because of the tidal interaction with the bulge of the Galaxy. The concentration of NGC 4833 is modest (c = 1.25, Harris 1996), and it is worth noting that the cluster has a very eccentric orbit ($e \sim 0.84$; Casetti-Dinescu et al. 2007) passing very close to the Galactic bulge. This is probably a lethal combination for a cluster.

We inserted the data for NGC 4833 (from Harris 1996; Casetti-Dinescu et al. 2007) in Eq. (2) of Dinescu et al. (1999) that estimates the inverse ratio of the destruction time due to bulge shocking. For NGC 4833 we derived a destruction time between 1 and 3×10^8 years. The exact value depends on the mass of the Galactic bulge, assumed to be 34×10^9 $M_\odot$ (Johnston et al. 1995), and on the velocity at the pericentre of the orbit, between 200 and 400 km s^{-1}. The estimate may increase by a factor 2.5 by adopting a pericentre distance of 0.9 kpc, at the upper boundary of the range considered by Casetti-Dinescu et al. (2007), instead of 0.7 kpc. When compared to the other GCs included in the sample of Dinescu et al. (1999), NGC 4833 shows particularly critical parameters, making it a good candidate to strong tidal stripping and destruction by the bulge. Our estimate is approximate, but these findings are supported by Allen et al. (2006, 2008), who found that NGC 4833 has the sixth highest destruction rate among the 54 GCs analysed by them.

Incidentally, the low value of the $(M/L)_V$ we found (Sect. 2.1) also supports the hint of a significant loss of stars from the cluster, since energy equipartition should have favoured the loss of low mass stars.

The location of NGC 4833 and NGC 288 on the $M_V - IQR$ diagram suggests that variations in cluster concentration c can explain the observed scatter, at least in part. In Fig. 16 we plotted the residuals around the $M_V - IQR$ correlation against the cluster concentration c. There is indeed a significant anti-correlation between these two quantities: the Pearson linear correlation coefficient is $r_p = 0.52$ that has a probability lower than 1% to be a random result. Of course, in this case it is better to use a bivariate analysis. The best fit is then

$$IQR = -0.16 - (0.14 \pm 0.04)M_V - (0.16 \pm 0.08)c. \quad (1)$$

The rms of residuals around this regression is 0.18, which compares well with typical internal errors in IQR[O/Na]. The correlation would further improve by excluding the core-collapse GCs, whose concentration is arbitrarily put at the constant value 2.5 in Harris (1996). The Pearson linear coefficient provided by this regression is $r_p = 0.65$. This result indicates that at a given absolute magnitude M_V, more loose clusters have a more extended Na-O anticorrelation than more compact ones. This might seem to contradict the observation that second-generation stars are more centrally concentrated than first-generation ones, at least in several clusters (Gratton et al. 2012, and references therein). However, this may well be explained if the real parameter driving the Na-O anticorrelation is the original rather than the present-day mass, and more loosely concentrated clusters have lost more mass than the more compact ones. The original mass of loosely concentrated clusters is therefore higher on average than for more compact clusters that now have the same M_V. More loose clusters are actually expected to be destroyed at a much faster rate by the tidal effects of the bulge and disk because the destruction rates for these mechanisms are expected to be proportional to the inverse of the cluster density (see Eqs. (1) and (2) in Dinescu et al. 1999).

If this argument is correct, IQR[O/Na] could be considered a better proxy for the original cluster mass than M_V. We might then possibly use the location of a cluster in the $M_V - IQR$ diagram to infer not only its original mass, but also the amount of mass lost (assuming that very compact clusters only lose a small fraction of their original mass). This is quite a speculative but interesting possibility, which should be compared to other dynamical indicators of mass loss, such as the slope of the mass function. We intend to make such a comparison in a future study.

6. Summary

In the extension of our FLAMES survey of Na-O anticorrelation in GCs (e.g. Carretta et al. 2009a,b), we analysed FLAMES data for 78 RGB member stars of NGC 4833 (73 observed with GIRAFFE, 12 with UVES, and 7 in common). This is the first massive high-resolution spectroscopic study of this cluster. We confirmed that it is a metal-poor GCs, with an average [Fe/H] $= -2.04 \pm 0.003$ from the 73 GIRAFFE stars and $= -2.015 \pm 0.004$ from the 12 UVES stars. The rms dispersion is very small (0.024 and 0.014 dex, respectively), making NGC 4833 one of the most homogenous GC, at least in its general metallicity.

We obtained abundances of Na and O and concluded that the cluster presents the typical Na-O anticorrelation found in (almost) all MW GCs (e.g. Carretta et al. 2010a; Gratton et al. 2012). The extension of the anticorrelation, as measured from the interquartile range of the [O/Na] ratio, is large. This is in line with the expectations based on its very extended HB. The limited sample of UVES stars shows a marked bimodality in Na and O abundances, as well as in Mg, Al, Si, with P and I,E stars clearly separated. The GIRAFFE sample only shows a hint of this separation, because of the larger errors in the abundances.

More exceptional is, however, the finding of large star-to-star variation in Mg abundance, anticorrelated with Al, Na, and Si. The strong depletion in Mg implies nuclear processing at very high temperatures, exceeding a threshold equal to about 65 million Kelvin (Arnould et al. 1999). This has been found to date only in a few cases, mostly metal-poor and massive GCs, with the more extreme changes seen in objects such as the very massive ω Cen, M 54, and NGC 2419 (and to a lesser degree in NGC 2808). With a metallicity similar to NGC 4833, NGC 2419 is a more extreme case and clearly a unique case among GCs in the Milky Way. However, NGC 4833 reaches Mg depletion similar to the other massive clusters mentioned above, and it stands out among GCs of similar low metallicity.

This unusual chemical pattern, coupled with the position of NGC 4833 in the relation between IQR[O/Na] and mass (total absolute magnitude), seems to indicate that the cluster was much more massive in the past. NGC 4833 has probably lost a conspicuous fraction of its original mass due to bulge shocking, as also indicated by its orbit.

Acknowledgements. We thank Chris Sneden for sending us the hyperfine structure components of many lanthanum lines, and we thank the referee for a careful reading of the manuscript and for suggestions. This publication makes use of data products from the Two Micron All Sky Survey, which is a joint project of the University of Massachusetts and the Infrared Processing and Analysis Center/California Institute of Technology, funded by the National Aeronautics and Space Administration and the National Science Foundation. This research has been funded by PRIN INAF 2011 "Multiple populations in globular clusters: their role in the Galaxy assembly" (PI E. Carretta), and PRIN MIUR 2010–2011, project "The Chemical and Dynamical Evolution of the Milky Way and Local Group Galaxies" (PI F. Matteucci). This research made use of the SIMBAD database, operated at the CDS, Strasbourg, France, and of NASA's Astrophysical Data System.

References

Allen, C., Moreno, E., & Pichardo, B. 2006, ApJ, 652, 1150
Allen, C., Moreno, E., & Pichardo, B. 2008, ApJ, 674, 237
Alonso, A., Arribas, S., & Martinez-Roger, C. 1999, A&AS, 140, 261
Alonso, A., Arribas, S., & Martinez-Roger, C. 2001, A&A, 376, 1039
Arnould, M., Goriely, S., & Jorissen, A. 1999, A&A, 347, 572
Bragaglia, A., Carretta, E., Gratton, R. G., et al. 2001, AJ, 121, 327
Bastian, N., Lamers, H. J. G. L. M., de Mink, S. E., et al. 2013a, MNRAS, 436, 2398
Bastian, N., Cabrera-Ziri, I., Davies, B., & Larsen, S. S. 2013b, MNRAS, 436, 2852
Bellazzini, M., Bragaglia, A., Carretta, E., et al. 2012, A&A, 538, A18
Cardelli, J. A., Clayton, G. C., & Mathis, J. S. 1989, ApJ, 345, 245
Carretta, E. 2006, AJ, 131, 1766
Carretta, E., Bragaglia, A., Gratton R. G., et al. 2006, A&A, 450, 523
Carretta, E., Bragaglia, A., Gratton, R.G., et al. 2007a, A&A, 464, 967
Carretta, E., Bragaglia, A., Gratton, R. G., Lucatello, & S. Momany, Y. 2007b, A&A, 464, 927
Carretta, E., Recio-Blanco, A., Gratton, R.G., Piotto, G., Bragaglia, A. 2007c, ApJ, 671, L125
Carretta, E., Bragaglia, A., Gratton, R. G., et al. 2009a, A&A, 505, 117
Carretta, E., Bragaglia, A., Gratton, R. G., & Lucatello, S. 2009b, A&A, 505, 139
Carretta, E., Bragaglia, A., Gratton, R. G., D'Orazi, V., & Lucatello, S. 2009c, A&A, 508, 695
Carretta, E., Bragaglia, A., Gratton, R. G., et al. 2010a, A&A, 516, A55
Carretta, E., Bragaglia, A., Gratton, R. G., et al. 2010b, A&A, 520, A95
Carretta, E., Bragaglia, A., Gratton, R., et al. 2010c, ApJ, 712, L21
Carretta, E., Lucatello, S., Gratton, R. G., Bragaglia, A., & D'Orazi, V. 2011, A&A, 533, A69
Carretta, E., Bragaglia, A., Gratton, R. G., Lucatello, S., & D'Orazi, V. 2012a, ApJ, 750, L14
Carretta, E., Gratton, R. G., Bragaglia, A., D'Orazi, V., & Lucatello, S. 2012b, A&A, 550, A34
Carretta, E., Bragaglia, A., Gratton, R. G., et al. 2013a, A&A, 557, A138
Carretta, E., Gratton, R. G., Bragaglia, A., et al. 2013b, ApJ, 769, 40
Casetti-Dinescu, D. I., Girard, T. M., Herrera, D., et al. 2007, AJ, 134, 195
Cohen, J. G., & Kirby, E. N. 2012, ApJ, 760, 86
Cohen, J. G., & Melendez, J. 2005, AJ, 129, 1607
D'Antona, F., Bellazzini, M., Caloi, V., et al. 2005, ApJ, 631, 868
Decressin, T., Meynet, G., Charbonnel, C., Prantzos, N., & Ekstrom, S. 2007, A&A, 464, 1029
Decressin, T., Baumgardt, H., & Kroupa, P. 2008, A&A, 492, 101
de Marchi, G., & Pulone, L. 2007, A&A, 467, 107
de Mink, S. E., Pols, O. R., Langer, N., & Izzard, R. G. 2009, A&A, 507, L1
Denisenkov, P. A., & Denisenkova, S. N. 1989, A. Tsir., 1538, 11
D'Ercole, A., Vesperini, E., D'Antona, F., McMillan, S. L. W., & Recchi, S. 2008, MNRAS, 391, 825
Dinescu, D. I., Girard, T. M., & van Altena, W. F. 1999, AJ, 117, 1792

D'Orazi, V., Biazzo, K., Desidera, S., et al. 2012, MNRAS, 423, 2789
D'Orazi, V., Campbell, S. W., Lugaro, M., et al. 2013, MNRAS, 433, 366
Figuera Jaimes, R., Arellano Ferro, A., Bramich, D. M., Giridhar, S., & Kuppuswamy, K. 2013, A&A, 556, A20
Garcia Lugo, G., Arellano Ferro, A., & Rosenzweig, P. 2007, IAU Symp, 240, 214
Gratton, R. G. 1988, Rome Obs. Preprint Ser., 29
Gratton, R. G., & Ortolani, S. 1989, A&A, 211, 41
Gratton, R. G., Carretta, E., Eriksson, K., & Gustafsson, B. 1999, A&A, 350, 955
Gratton, R. G., Sneden, C., Carretta, E., & Bragaglia, A. 2000, A&A, 354, 169
Gratton, R. G., Carretta, E., Claudi, R., Lucatello, S., & Barbieri, M. 2003, A&A, 404, 187
Gratton, R. G., Sneden, C., & Carretta, E. 2004, ARA&A, 42, 385
Gratton, R. G., Lucatello, S., Bragaglia, A., et al. 2006, A&A, 455, 271
Gratton, R. G., Lucatello, S., Bragaglia, A., et al. 2007, A&A, 464, 953
Gratton, R. G., Carretta, E., & Bragaglia, A. 2012, A&ARv, 20, 50
Harris, W. E. 1996, AJ, 112, 1487
Johnson, C. I., & Pilachowski, C. A. 2010, ApJ, 722, A1373
Johnson, C. I., & Pilachowski, C. A. 2012, ApJ, 754, L38
Johnston, K. V., Spergel, D. N., & Hernquist, L. 1995, ApJ, 451, 598
Kains, N., Bramich, D. M., Arellano Ferro, A., et al. 2013, A&A, 555, A36
Kaluzny, J., Olech, A., Thompson, I., et al. 2000, A&AS, 143, 215
Karakas, A. I., & Lattanzio, J. C. 2003, PASA, 20, 279
King, I. R. 1966, AJ, 71, 64
Kraft, R. P., & Ivans, I. I. 2003, PASP, 115, 143
Landolt, A. U. 1992, AJ, 104, 340
Langer, G. E., Hoffman, R., & Sneden, C. 1993, PASP, 105, 301
Leon, S., Meylan, G., & Combes, F. 2000, A&A, 359, 907
Maccarone, T. J., & Zurek, D. R. 2012, MNRAS, 423, 2
Mackey, A. D., & van den Bergh, S. 2005, MNRAS, 360, 631
Magain, P. 1984, A&A, 134, 189
Manfroid, J., Selman, F., & Jones, H. 2001, The Messenger, 104, 16
Martin, N. F., Ibata, R. A., Chapman, S. C., Irwin, M. J., & Lewis, G. F. 2007, MNRAS, 380, 281
Melbourne, J., & Guhathakurta, P. 2004, AJ, 128, 271
Melbourne, J., Sarajedini, A., Layden, A., & Martins, D. H. 2000, AJ, 120, 3127
Milone, A., Piotto, G., Bedin, L., et al. 2012, ApJ, 744, 58
Milone, A. P., Marino, A. F., Piotto, G., et al. 2013, ApJ, 767, 120
Minniti, D., Peterson, R. C., Geisler, D., & Claria, J. J. 1996, ApJ, 470, 953
Momany, Y., Bedin, L. R., Cassisi, S., et al. 2004, A&A, 420, 605
Mucciarelli, A., Bellazzini, M., Ibata, R., et al. 2012, MNRAS, 426, 2889
Murphy, B. W., & Darragh, A. N. 2012, J. South Eastern Assoc. Res. Astron., 6, 72
Murphy, B. W., & Darragh, A. N. 2013, AAS Meeting #222, #115.12
Norris, J. E., & Da Costa, G. S. 1995, ApJ, 441, L81
Pasquini, L., Avila, G., Blecha, A., et al. 2002, The Messenger, 110, 1
Paust, N. E. Q., Reid, I. N., Piotto, G., et al. 2010, AJ, 139, 476
Piotto, G., King, I. R., Djorgovski, S. G., et al. 2002, A&A, 391, 945
Piotto, G., Bedin, L., Anderson, J., et al. 2007, ApJ, 661, L53
Prantzos, N., Charbonnel, C., & Iliadis, C. 2007, A&A, 470, 179
Pryor, C., & Meylan, G. 1993, ASP Conf. Ser., 50, 357
Ramirez, S., & Cohen, J. G. 2002, AJ, 123, 3277
Ramirez, S., & Cohen, J. G. 2003, AJ, 125, 224
Recio-Blanco, A., Aparicio, A., Piotto, G., De Angeli, F., & Djorgovski, S. G. 2006, A&A, 452, 875
Simmerer, J., Sneden, C., Ivans, I. I., et al. 2003, AJ, 125, 2018
Skrutskie, M. F., Skrutskie, M. F., Cutri, R. M., Stiening, R., et al. 2006, AJ, 131, 1163
Sneden, C., Cowan, J. J., Lawler, James, E., et al. 2003, ApJ, 591, 936
Sobeck, J. S., Ivans, I. I., Simmerer, J. A., et al. 2006, AJ, 131, 2949
Sollima, A., Bellazzini, M., & Lee, J.-W. 2012, ApJ, 755, 156
Stetson, P. B. 1994, PASP, 106, 250
Valcarce, A. A. R., & Catelan, M. 2011, A&A, 533, A120
Valdes, F. G. 1998, Astronomical Data Analysis Software and Systems VII, eds. R. Albrecht, R. N. Hook, & H. A. Bushouse, ASP Conf. Ser., 145, 53
Venn, K. A, Irwin, M., Shetrone, M. D., Tout, C. A., Hill, V., & Tolstoy, E. 2004, AJ, 128, 1177
Ventura, P., D'Antona, F., Mazzitelli, I., & Gratton, R. 2001, ApJ, 550, L65
Ventura, P., D'Antona, F., Di Criscienzo, M., et al. 2012, ApJ, 761, L30
Worley, C. C., Hill, V., Sobeck, J., & Carretta, E. 2013, A&A, 553, A47
Yong, D., Grundahl, F., Nissen, P. E., Jensen, H. R., & Lambert, D. L. 2005, A&A, 438, 875
Yong, D., Mélendez, J., Grundahl, F., et al. 2013, MNRAS, 434, 3452

Astronomy & Astrophysics: a European journal

BACK TO RESULTS

Basic Description | Other Editions/ Formats | Abstracting/ Indexing & Article Access | Publisher & Ordering Information | Advertising, Rights, Demographics | Reviews

JCR Web

Click highlighted text for a new search on that item.

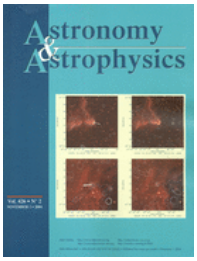

Table of Contents:	Click here to view
ISSN:	0004-6361
Title:	Astronomy & Astrophysics: a European journal
Publishing Body:	E D P Sciences
Country:	France
Status:	Active
Start Year:	1930
Frequency:	48 times a year
Annual Term:	In 16 vols; 3 nos. per vol.
Volume Ends:	# 3,
Document Type:	Journal; Academic/Scholarly
Refereed:	Yes
Abstracted / Indexed:	Yes
Media:	Print
Alternate Edition ISSN:	1432-0746
Language:	Text in English
Price:	EUR 3,650 combined subscription per year in the European Union to individuals (Print & Online Eds.) EUR 3,750 combined subscription per year elsewhere to institutions (Print & Online Eds.) (effective 2010)
Subject:	ASTRONOMY PHYSICS
Dewey #:	520, 523.01
LC#:	QB1
CODEN:	AAEJAF
Special Features:	Includes Advertising, Bibliographies, Charts, Illustrations
Article Index:	Index, cum.index
URL:	http://www.edpsciences.org
Description:	Presents papers on all aspects of astronomy and astrophysics - theoretical, observational, and instrumental - regardless of the techniques used - optical, radio, particles, space vehicles, and numerical analysis.

Additional Title Information

ADDITIONAL TITLE INFORMATION

Title History: Superseded in part (in 1968): Zeitschrift fuer Astrophysik (Germany) (0372-8331); Incorporated (1947-1992): Astronomical Institutes of Czechoslovakia. Bulletin (Czech Republic) (0004-6248); (1966-2000): Astronomy & Astrophysics. Supplement Series (France) (0365-0138); Which was formerly (until 1970): Astronomical Institutes of the Netherlands. Bulletin. Supplement Series (Netherlands) (0365-8910); Which incorporated (1900-1960): Kapteyn Astronomical Laboratory at Groningen. Publications (Netherlands) (0927-3107); Which was formerly (until 1924): Astronomical Laboratory at Groningen. Publications (Netherlands) (0929-6255)

Back to Top

Add this item to: (select a list) + ADD

Request this title: I'd like to request this title. GO

Corrections: Submit corrections to Ulrich's about this title. GO

Publisher of this title? If yes, click GO! to contact Ulrich's about updating your title listings in the Ulrich's database. GO

• Print • Download • E-mail

Back to Top